Int. J. Electrochem. Sci., 11 **(2016)** 10561 – 10580, doi: 1020964/2016.12.75

International Journal of ELECTROCHEMICAL SCIENCE
www.electrochemsci.org

Effect of Heat Treatment on Stress Corrosion Cracking Behavior and Electrochemical Characteristic of Welded Ti-6Al-4V Alloy during Slow Strain Rate Test

Yan Liu[1], *Shawei Tang*[1], *Guangyi Liu*[1,2], *Yue Sun*[1], *Jin Hu*[1,*]

[1] School of Materials Science and Engineering, Harbin Institute of Technology, Harbin 150001, China
[2] State Key Laboratory for Marine Corrosion and Protection, Luoyang Ship Material Research Institute (LSMRI), Qingdao 266101, China
[*]E-mail: hujin@hit.edu.cn

Received: 13 September 2016 / *Accepted:* 11 October 2016 / *Published:* 10 November 2016

Local rapid induction heating is used as a post weld heat treatment for a welded Ti-6Al-4V alloy. The welded sample is heat treated at different temperatures. The microstructure and corrosion behavior of the welded sample before and after the post weld heat treatment are investigated. Electrochemical impedance spectroscopy (EIS) measurements under slow strain rate test (SSRT) are performed in a LiCl-methanol solution. The results demonstrate that the microstructure in fusion zone evolves from acicular α′ martensite phase in the as-welded sample to lathy α phase and transformational β phase in the heat treated samples. The lathy α phase decreases and the transformational β phase increases with the increase of the heat treatment temperature in the fusion zone. The mechanical properties and corrosion resistance of the welded samples are significantly improved after the heat treatment and gradually increase with the increase of the heat treatment temperature, which indicate that the post weld heat treatment effectively reduces the susceptibility of the welded Ti-6Al-4V alloy to stress corrosion cracking.

Keywords: Ti-6Al-4V alloy; Welding; Post weld heat treatment; Stress corrosion cracking; Electrochemical impedance spectroscopy; slow strain rate test

1. INTRODUCTION

Ti-6Al-4V alloys have been considered as the important structural material due to the excellent mechanical properties, corrosion resistance and chemical compatibility [1-5].

Because of the formation of a protective oxide film (TiO2) on the surface, titanium alloys are immune to many aggressive environments which induce corrosion behavior of conventional metallic materials such as aluminium alloys and steels [6-8]. Nevertheless, the protective oxide film can be

ruptured by external condition such as abnormal mechanical loads, erosion environments and their synergistic effects [9]. The stress corrosion cracking is a well known process of continuous performance deterioration. Under the combined action of stress and corrosion, crack propagation rate in a material can often be accelerated which leads to failure of structures. Usually, the applied stress caused stress corrosion cracking is much less than the yield strength of materials. The stress corrosion cracking behavior of titanium alloys in various aggressive environments such as organic solvent, aqueous solution, hot salt and even ionic liquid have been extensively investigated. For instance, Trasatti reported that the effect of the water content on the stress corrosion cracking susceptibility of pure titanium in *n*-propanol and *iso*-propanol solutions [10]. Pustode found a critical temperature for the initiation of stress corrosion cracking of Ti-6A1-2Sn-4Zr-2Mo-0.1Si alloy in hot salt [11]. Tsai found that the Ti–6Al–4V alloy was susceptible to stress corrosion cracking in Lewis-neutral aluminium chloride–1-ethyl-3-methylimidazolium chloride ionic liquid [12]. Titanium and its alloys have been proven to be susceptible to stress corrosion cracking in a series variety of application environments.

With the exploitation and application of Ti-6Al-4V alloys, welding are widely utilized [13-15]. The welding process has been considered to be harmful to the corrosion behavior of welded titanium alloys. Karimzadeh and Heidarbeigy found that the fusion zone of gas tungsten arc welding Ti–6Al–4V alloy showed lower corrosion resistance compared with the base metal in Ringer solution, which was indicated by the more negative corrosion potential and higher corrosion current densities [16,17]. Han reported the corrosion behavior of scanning electron beam welded Ti–6Al–4V alloy in acid CuSO4 solution and obtained the similar conclusions [18]. In conclusion, the fusion zone was considered to be particularly sensitive to corrosion and stress corrosion cracking because of the entirely different structure in comparison to the base metal. Our previous study showed that the welded Ti–6Al–4V alloy had stronger corrosion tendency and higher stress corrosion cracking susceptibility compared with the non-welded one in a chloride -methanol solution [19].

Hence, it is essential to suppress the stress corrosion cracking behavior for ensuring the reliabilities of the welded titanium alloys in the working environments during their service lives. Microstructure is an important factor that affects stress corrosion cracking behavior [20,21]. Several researches have indicated that the microstructure of welded titanium alloys could be adjusted by post weld heat treatment in past decades, such as bulk heat treatment in furnace [22-24]. However, the bulk heat treatment technologies are not suitable for large scale components because of the volume. Local heat treatment technology could be free from the limitation of volume and shape of the workpiece. Induction heating technology is a mature heat-treatment technology, which can provide a very fast heating speed for the workpieces. Particularly, the induction heating can produce a less deformation to the workpieces. The system generates a high-frequency alternating current passing through the induction coil. The flow of the alternating current induces a high-intensity and rapidly changing alternating magnetic field around the induction coil. The workpiece is placed in this alternating magnetic field and the rapid variation of alternating magnetic field produce an induction current flowing in the workpiece (according to the Faraday law of electromagnetic induction). The conductive workpiece could be heated by the joule heat which generate from the flow of induction current [25].

Induction heating technology has been proven to be efficient and applicable in titanium processing industry compare with the traditional convective or radiant heating technology [26-29].

Electrochemical impedance spectroscopy (EIS) has been proven to be effective to study the characteristics of the electrochemical corrosion and the process of electrodes reaction, which has been widely used in various materials [30-32]. To the author′ s knowledge, electrochemical impedance spectroscopy has been used in combination with slow strain rate test to study the stress corrosion cracking behavior of steel and aluminum, but very little researches reported on the titanium alloy, especially the relevant research on the welded titanium alloy is still very lacking [33-35]. Some researchers found that the heat treatment can affect the microstructures of welded samples [22-24], however, not much information is available regarding their influence on the electrochemical corrosion and stress corrosion cracking behavior. Therefore, the aim of the present paper is to adjust the microstructure of the welded Ti-6Al-4V alloy by post weld local rapid induction heating, in order to investigate the effect of heat treatment on the susceptibility of stress corrosion cracking and the electrochemical corrosion behavior.

2. EXPERIMENTAL

2.1 Materials and welding

Commercially available mill-annealed Ti–6A1–4V alloy sheet with dimensions of 240mm×50mm×1mm was prepared for laser welding in this work. The chemical composition of Ti–6A1–4V alloy was shown in Table 1.

Table 1. Chemical compositions (wt.%) of Ti–6A1–4V alloy.

Element	Ti	Al	V	Fe	C	O	H	N
Content	Balance	5.9	4.0	0.08	0.02	0.1	0.002	0.3

Ti–6A1–4V alloy were welded by using a Rofin-DC030 3kW laser beam system and the welding parameters was listed in Table 2. The surfaces of all samples were brushed and cleaned with acetone to remove contaminants and surface oxides before the welding. Pure argon was employed for avoiding oxidation of the workpiece in ambient gases.

Table 2. Parameters of the laser beam welding.

Power (W)	Frequency (Hz)	Welding speed（m/min）	Argon pressure (MPa)
800	35	1	0.12

2.2. Post weld local rapid induction heating

The control of microstructures of the weldments was carried out using post weld local rapid induction heating method.

The induction power supply was 60kW and the frequency was 25kHz. The induction coil was employed to scan the weld zone (reciprocating moving). Temperature was measured and controlled by utilizing an infrared thermometer focused on the surface of workpiece. The induction coil was located above the workpiece and the heating width was 20 mm. At the end of the heat treatment, the power supply was turned off and the workpiece cooled to room temperature. The schematic diagram of the heat treatment was shown in Figure 1 (the black arrow represented the moving direction of the workpiece) and the heating parameters was shown in Table 3.

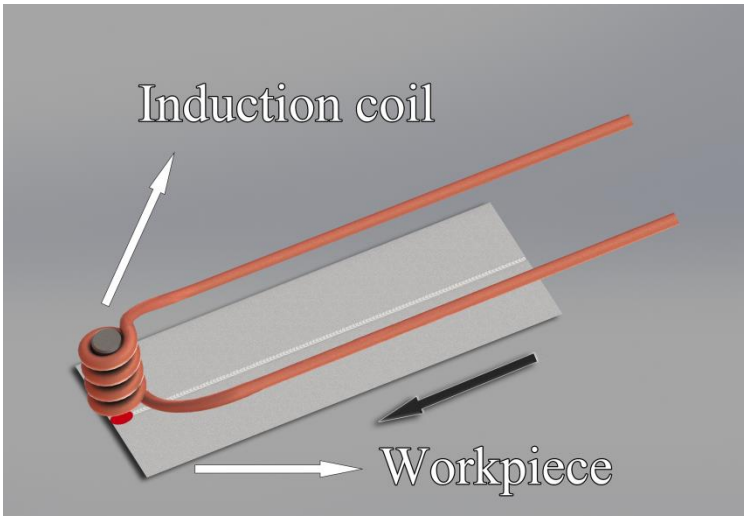

Figure 1. Schematic diagram of the post weld local rapid induction heating.

Table 3. Parameters of the post-weld local rapid induction heating.

Mode	Temperature (℃)	Scanning speed (mm/min)	Cyclic number	Abbreviation
Reciprocating scanning	500	120	15	H-500
	600			H-600
	700			H-700

2.3. Slow strain rate test

Titanium alloy has been proven to be susceptible to corrosion in organic medium such as methanol solution under the existence of applied stress, particularly the presence of chloride as LiCl [8]. The stress corrosion cracking susceptibility was assessed by slow strain rate test (LETRY WDL-1000) at a strain rate of 3×10-7 /s in 0.1 mol/L LiCl-methanol solution at room temperature. The

geometry of the tensile sample was shown in Figure 2. The tensile samples were covered with silicone rubber, the fusion zone with an area of 0.12 cm^2 was exposed to the test solution.

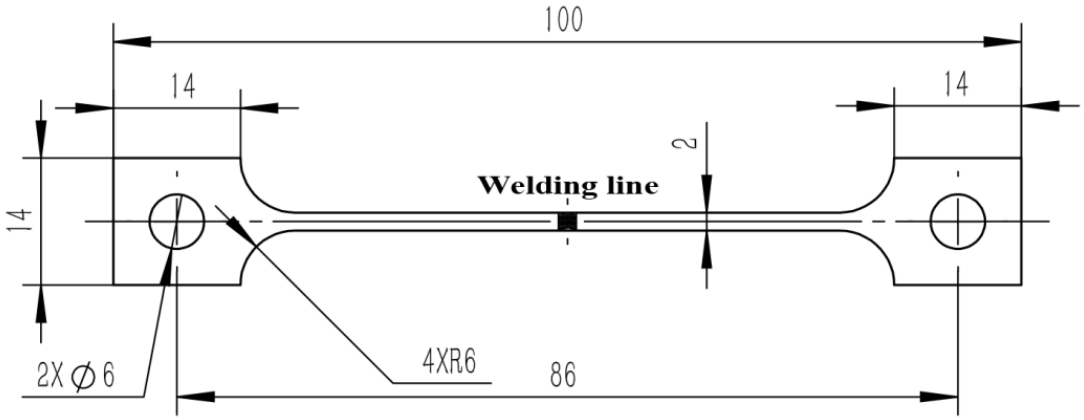

Figure 2. Dimensions of the tensile specimen, mm.

2.4. Electrochemical measurement

Stress corrosion cracking behavior was studied by using the slow strain rate test coupled with the electrochemical measurements. Electrochemical impedance spectroscopy was carried out through Gamry Reference 3000 electrochemical measurement system. Three-electrode cell was used in this study: a silver/silver chloride/methanol electrode [36-40] was used as the reference electrode, the tensile samples were used as the working electrode and the graphite was used as the counter electrode. Electrochemical impedance spectroscopy measurements were performed every 2h from the start of the slow strain rate test to the failure of the sample. A sinusoidal perturbation signal with amplitude of 10 mV was applied to the work electrode at the open circuit potential and the measuring frequency swept from 100 kHz to 0.01 Hz. The EIS results were analyzed by fitting the experimental data with ZSimpWin software.

2.5. Microstructure and fracture surface analysis

The samples were cross cut transverse to the welding direction. The cross-sections were ground, polished and etched using Kroll's solution for the microstructure analysis by light microscope (Olympus PMG2).

The phase composition of the samples was identified by X-ray diffraction (Philips, X'pert) using Cu Kα radiation source working at 40 kV and 40 mA. The scanning range was from 30° to 70° with scanning rate of 0.1 °/s.

The fracture analysis of the tensile samples was performed by Hitachi S-3000N scanning electron microscope.

3. RESULTS AND DISCUSSION

3.1 Microstructures of the welded Ti-6Al-4V alloy before and after heat treatment

Figure 3 exhibits the typical microstructure of the as-welded Ti-6Al-4V alloy. As shown in Figure 3a, the base metal is found to be composed of a bright equiaxed α phase (hexagonal close-packed structure) and a dark β phase (body-centered cubic structure), the β phase distributes at the α phase boundaries.

Titanium and its alloys have the behaviors of the reversible transformation, when the temperatures reach a certain level, the phase structures completely change from a hexagonal close-packed structure (α phase) to a body-centered cubic structure (β phase). The transformation temperatures are influenced by the kinds and content of the alloying elements. For the Ti-6Al-4V alloy, the transformation temperature is approximately 985℃ which is known as the β transition temperature. Though, the temperature exceeds the melting point of the Ti-6Al-4V alloy during the welding process. There is no enough time for the β phase to transform into the α equilibrium phase through diffusion transformation because of the high cooling speed during the solidification process. Conversely, a diffusionless transformation from the β phase to the martensite solidification structure occurs through the regular migration of atoms in β phase. The fine acicular α′ martensite solidification structure (supersaturated nonequilibrium hexagonal phase) with the different crystallographic orientations within the coarse prior β columnar grains (epitaxially grows along the direction from the semi-melted β grains near the fusion boundary to the weld centerline) is observed in the fusion zone, as shown in Figure 3b. The boundaries of the prior β columnar grains are clear. The microstructure of the fusion zone corresponds to that of Ti-6Al-4V alloy quenches from β phase region above the β transition temperature. The microstructure of the heat affected zone contains some different features which are not observed in the fusion zone. On the basis of the different microstructures, the heat affected zone is usually divided into two subregions, the heat affected zone close to the fusion zone (near-heat affected zone) and the heat affected zone close to the base metal (far-heat affected zone). As shown in Figure 3c, the microstructure of the near-heat affected zone is made of the acicular α′ martensite phase. In the near-heat affected zone, the peak temperature surpasses the β transition temperature in the process of welding. The near-heat affected zone could be considered as the fully transformed region, thus, the microstructure of the near-heat affected zone is similar to that of the fusion zone. The microstructure of the far-heat affected zone includes the acicular α′ martensite phase, the original α phase and the original β phase, as shown in Figure 3d. For the far-heat affected zone, the driving force of the transformation is low due to the peak temperature which is below the β transition temperature. The appearance of the remaining original α phase and original β phase indicates the incomplete transformation from the β phase to the α′ martensite phase, thus, the far-heat affected zone could be considered as the partially transformed region. From the near-heat affected zone to the far-heat affected zone, the amount of the acicular α′ martensite phase decreases with the increasing in the amounts of the original α phase and the original β phase, which leads to a great gradient of the microstructure in the heat affected zone. The microstructure of the welded Ti–6A1–4V alloy has been investigated by many researches which showed the similar microstructure of the fusion zone (acicular

α′ martensite phase), near-heat affected zone (acicular α′ martensite phase) and far-heat affected zone (acicular α′ martensite phase, original α phase and original β phase) from the welded Ti–6A1–4V alloy [13-15]. The microstructure of the welded Ti–6A1–4V alloy was also discussed in our previous research [19].

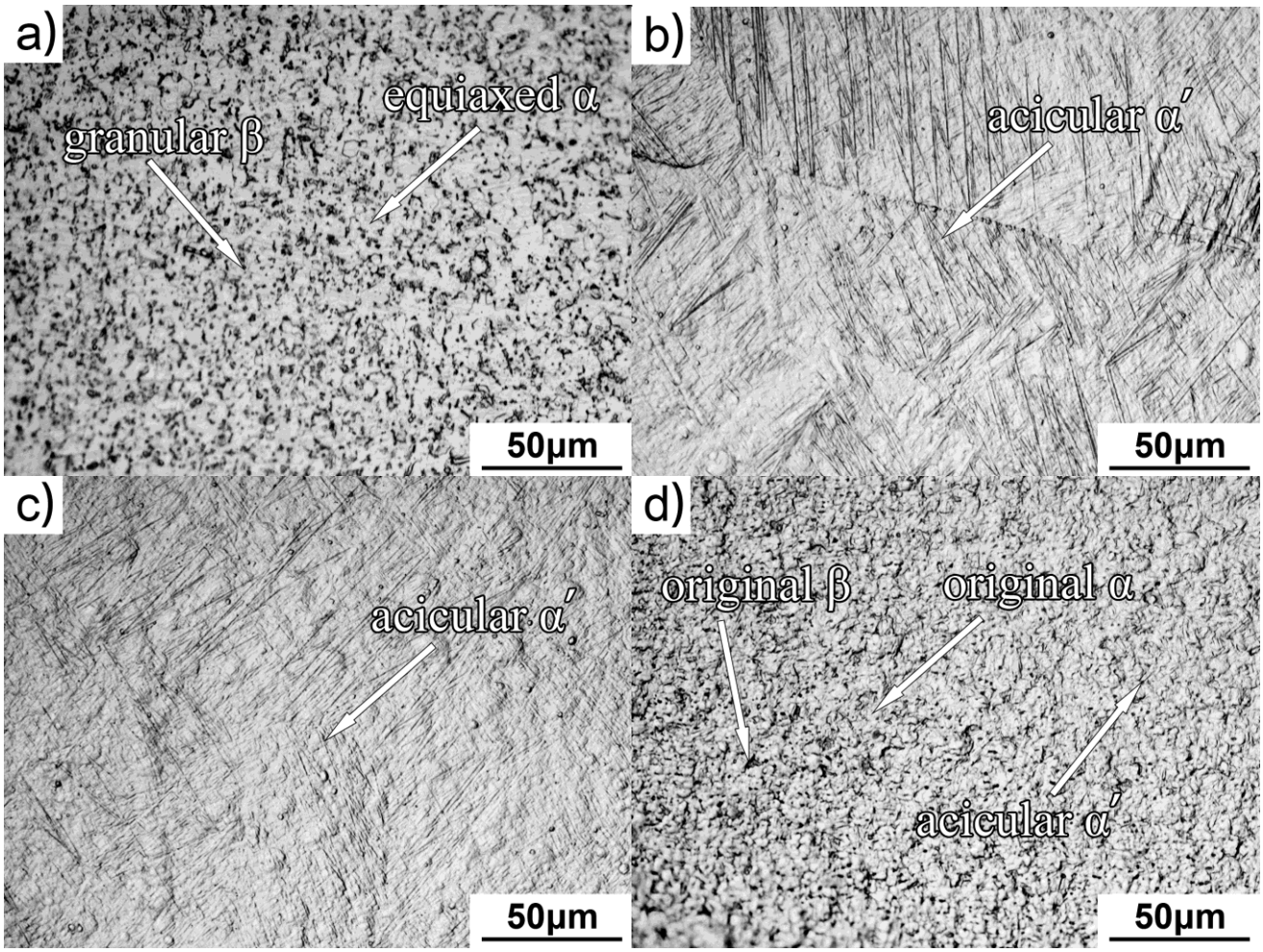

Figure 3. Microstructure of the welded Ti-6Al-4V alloy: (a) base metal; (b) fusion zone; (c) near-heat affected zone; (d) far-heat affected zone.

Figure 4 presents the XRD patterns of the fusion zones in the welded samples before and after the heat treatment. Only α′ martensite phase existed at the as-welded sample. The diffraction peaks of the welded samples are made of α phase and β phase together after heat treatment. It is clearly shown that the phase transformation: $\alpha' \rightarrow \alpha + \beta$ occurs during the process of the post weld local rapid induction heating, and the heat treatment temperature does not change the phase compositions of the fusion zones in the welded samples.

Figure 5 displays the images of the fusion zones for the welded samples after the heat treatment with the different temperatures. It can be found that the microstructure of the heat treated samples is similar no matter what the heat treatment temperature is, as shown in Figure 5a, Figure 5c and Figure 5e.

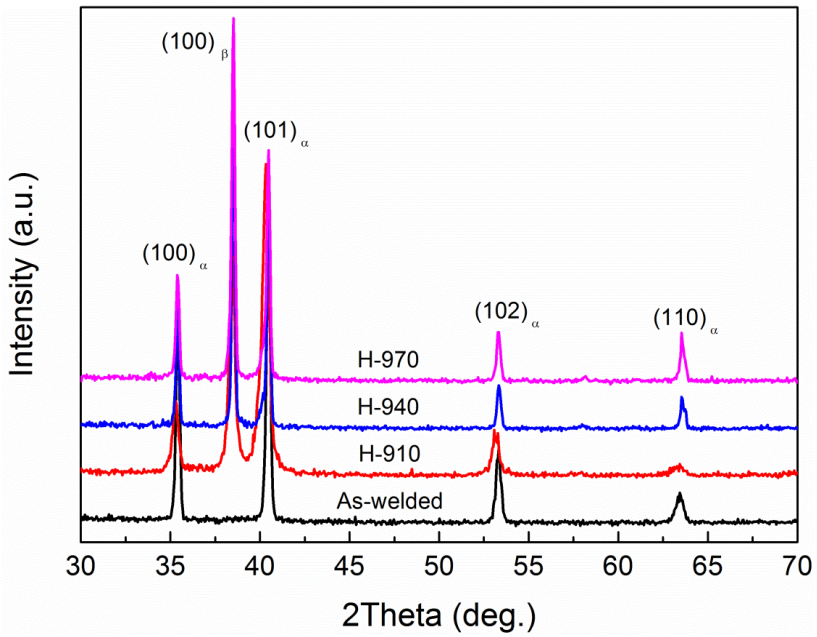

Figure 4. XRD patterns of the fusion zones of the as-welded samples with and without heat treatment.

According to the XRD results, the acicular α′ martensite phases presented in the fusion zones of the as-welded sample are transformed into α phases and β phases after the post weld heat treatment. Thus the bright lathy α phases and the dark transformed β phases exist together in the heat treated samples. Similar results have been found by other author. Thomas et al. reported that the phase composition of the fusion zone in the welded Ti-6Al-4V alloy after heat treatment was almost similar to that in the as-welded sample when the heat treatment temperature was in a relatively low level such as 540 ℃, they are consisted of α′ martensite phases [41]. But the α′ martensite phase was transformed into lathy α phases and β phases, the transformed β phases presented at the α phases interface after heat treatment in a relatively high temperature such as 950 ℃, and the microstructural evolution was also observed by Kabir et al. after the samples underwent heat treatment in a similar temperature (538 ℃ and 913 ℃) for the welded Ti-6Al-4V alloy [22,23].

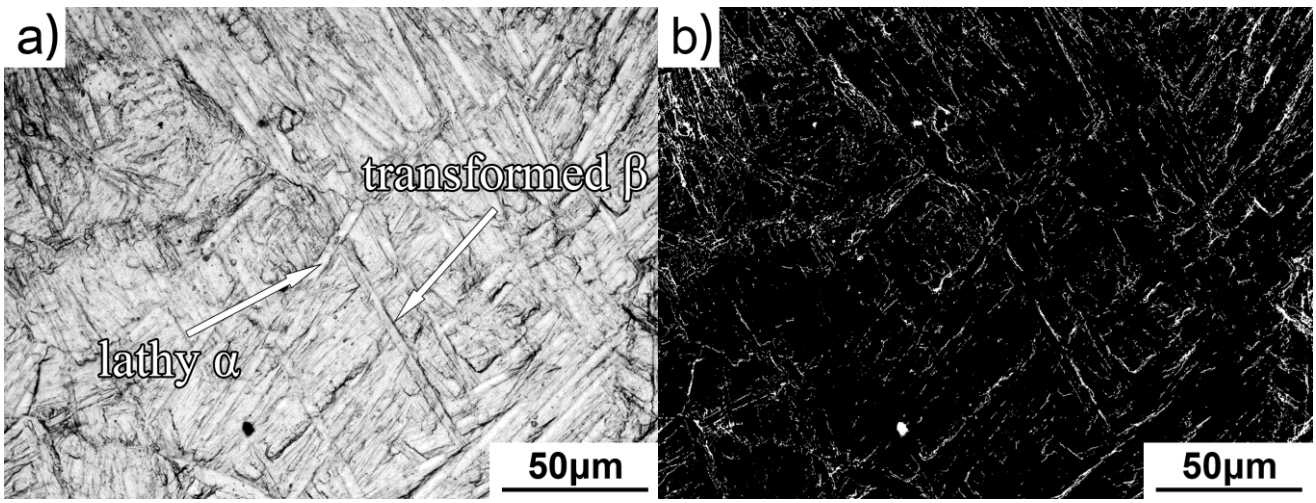

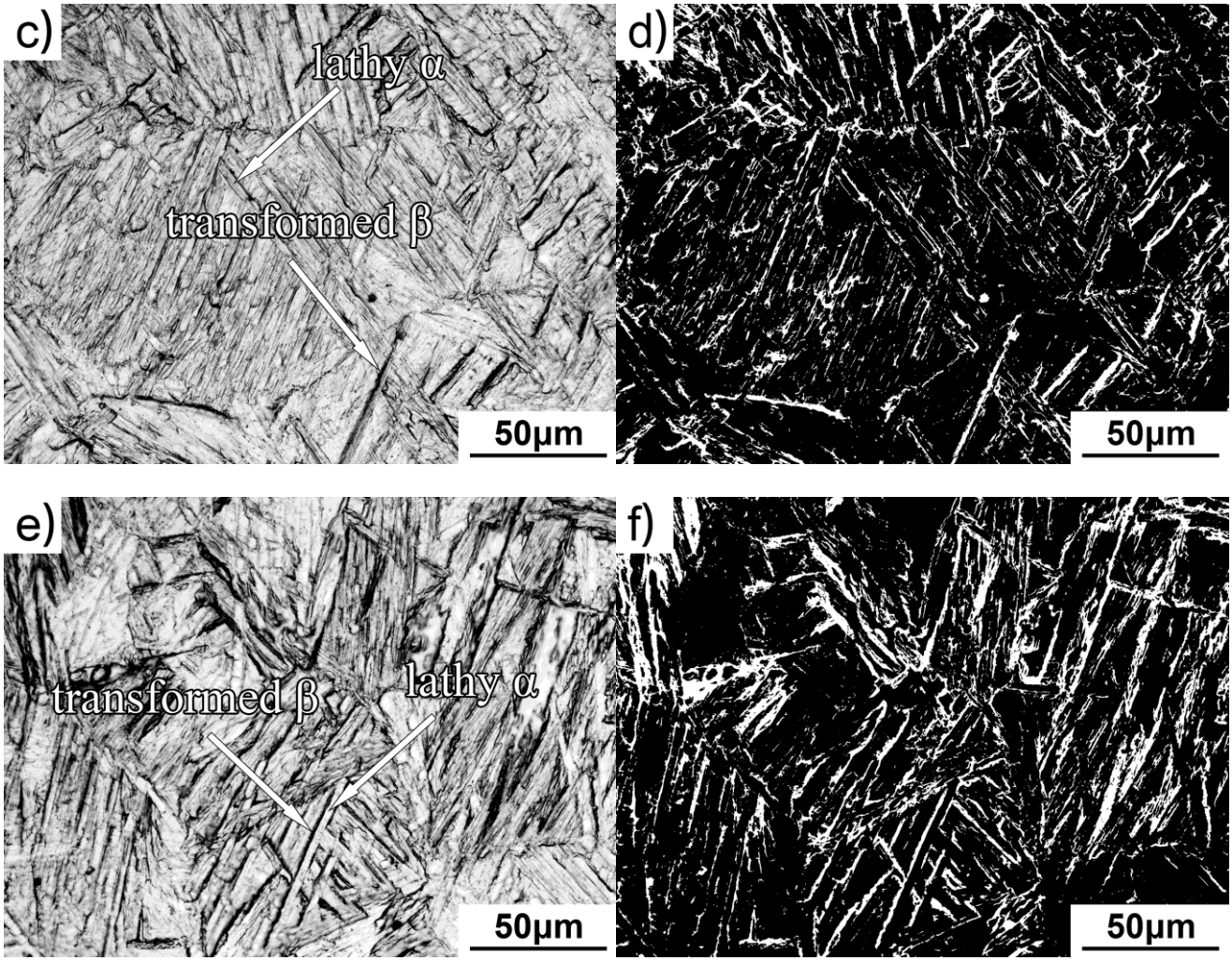

Figure 5. Microstructures of the fusion zones in the welded Ti-6Al-4V alloy after post weld heat treatment with the different temperatures: (a) 910 ℃ treated sample; (b) monochromatic photographs of Fig. 5a; (c) 940 ℃ treated sample; (d) monochromatic photographs of Fig. 5c; (e) 970 ℃ treated sample; (f) monochromatic photographs of Fig. 5e.

The black and white monochromatic photographs of Figure 5a, Figure 5c and Figure 5e transformed by using software of "Image Pro Plus" are shown in Figure 5b, Figure 5d and Figure 5f. In the monochromatic photographs, the black area represents the lathy α phase and the white area represents the transformed β phase. It is seen that the content of the transformed β phase obviously increase with the heat treatment temperature, which implies the decreasing content of the lathy α phase.

3.2. Slow strain rate test

The method of slow strain rate test is employed in order to examine the susceptibility of the heat treated samples to stress corrosion cracking [42-45]. Figure 6 displays the stress-strain curves of

the welded samples before and after the heat treatment during the slow strain rate test process in corrosive medium and air. The detailed mechanical properties, such as the breaking elongation and the ultimate tensile strength are summarized in Table 4, the susceptibility of the welded sample before and after heat treatment to stress corrosion cracking can be evaluated by comparing their mechanical properties.

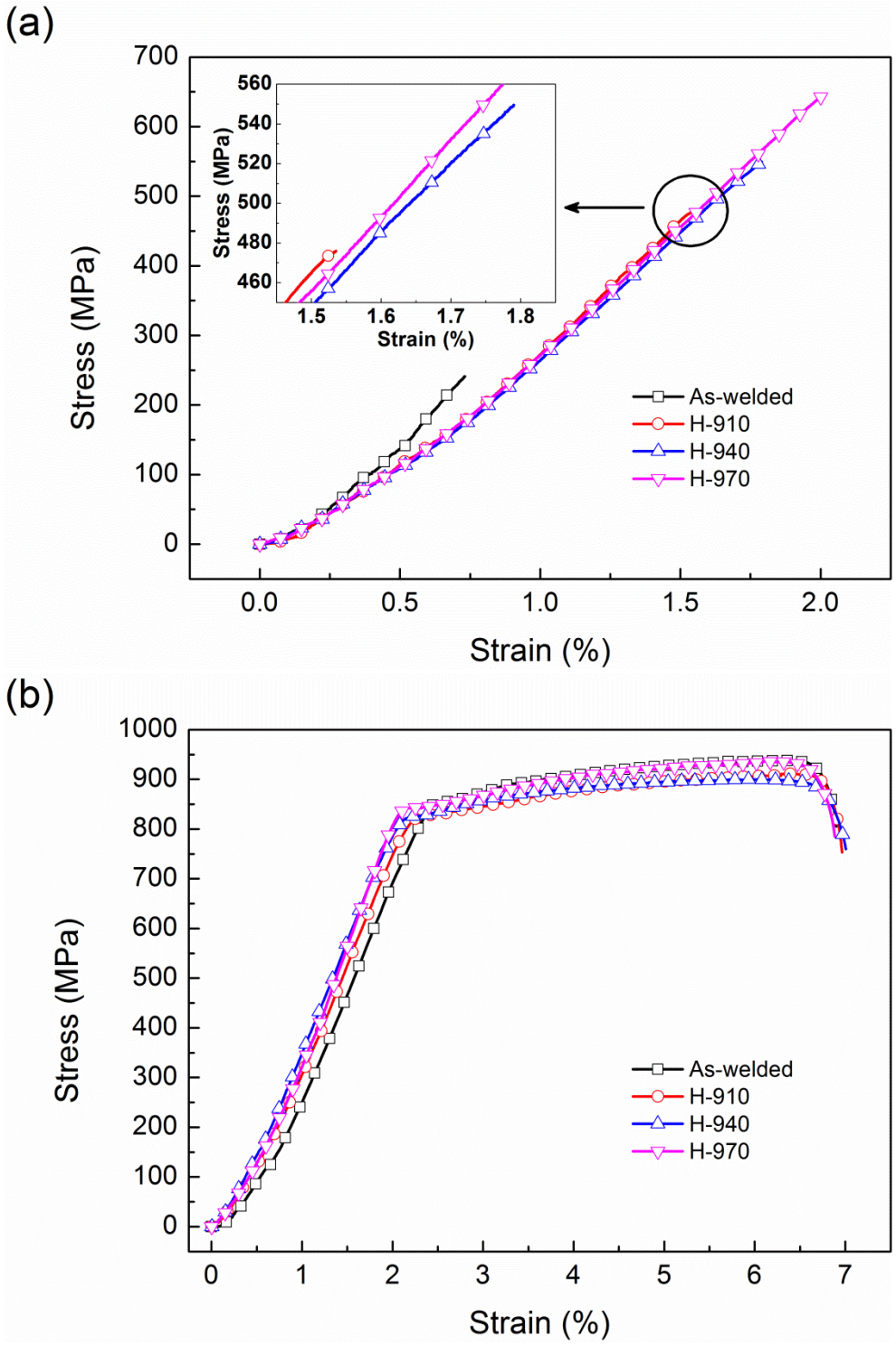

Figure 6. Stress-strain curves of the welded samples before and after post weld heat treatment during the slow strain rate test process: (a) tested in solution; (b) tested in air.

The results from Figure 6 and Table 4 present that the ultimate tensile strength and the breaking elongation for the as-welded sample are only 241 MPa and 0.73%, respectively. The poor mechanical properties imply the high susceptibility to stress corrosion cracking. To the Ti-6Al-4V alloy, Yin et al. reported the similar cracking behavior in methanol solution and air under slow strain rate test, who found that the mechanical properties such as the breaking elongation obtained from methanol solution significantly decreased compared with that tested in air condition, the breaking elongation of the sample decreased by 52% [46]. It can be clearly seen that there are obvious improvement in the mechanical properties of the welded samples after heat treatment. The ultimate tensile strength and the breaking elongation of the heat treated samples obviously increase with the heat treatment temperature. In comparison with the as-welded sample, the ultimate tensile strength and the breaking elongation of the sample heat treated at 970 ℃ increase by 168 % and 175 %, respectively.

The susceptibility index of stress corrosion cracking can be expressed by the loss ratio of mechanical properties through the comparison of the samples tested in corrosive medium and air, such as the loss ratio in ultimate tensile strength (I_σ) and breaking elongation (I_ε), as following equations show:

$$I_\sigma\ (\%) = \frac{\sigma_{air} - \sigma_{sol}}{\sigma_{air}} \times 100 \quad (1)$$

$$I_\varepsilon\ (\%) = \frac{\varepsilon_{air} - \varepsilon_{sol}}{\varepsilon_{air}} \times 100 \quad (2)$$

Where σ_{air} and ε_{air} represent the ultimate tensile strength and the breaking elongation obtained in air, σ_{sol} and ε_{sol} represent the ultimate tensile strength and the breaking elongation obtained in solution [47-49]. To the titanium alloy, Wu et al. found that the susceptibility index of stress corrosion cracking tested in methanol solution reached up to 92.5% compared with that which was 0% obtained from air condition [50]. According to the mechanical properties shown in Table 4, the susceptibility index I_σ and I_ε can be obtained, as shown in Figure 7. It can be seen that the susceptibility index of the stress corrosion cracking significantly decreases after the heat treatment, the higher heat treatment temperature implies the lower susceptibility index. It is without question, the post weld heat treatment effectively reduces the susceptibility of the welded Ti-6Al-4V alloy to stress corrosion cracking in LiCl-methanol solution.

Table 4. Tensile data of the samples from Fig. 6

Sample	Condition	Ultimate tensile strength (MPa)	Breaking elongation (%)
A-welded	Solution	241	0.73
	Air	938	6.89
H-910	Solution	476	1.54
	Air	911	6.96
H-940	Solution	550	1.79
	Air	900	7.01
H-970	Solution	646	2.01
	Air	935	6.88

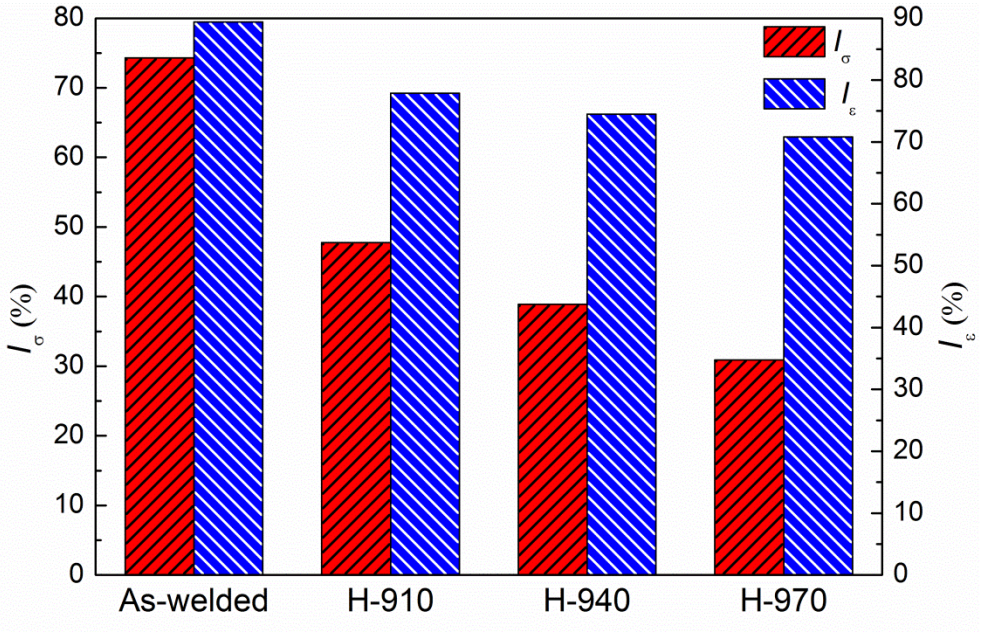

Figure 7. Susceptibility index of the stress corrosion cracking of the welded samples before and after post weld heat treatment.

The fractograph morphologies of the as-welded and heat treated samples tested in air and solution are displayed in Figure 8. As Figure 8a, Figure 8c, Figure 8e and Figure 8g show, the fracture mode of all the samples tested in solution is dominated by the brittle fracture due to the transgranular cleavage plane on the fracture surfaces [51]. For the samples tested in air, there are numerous dimples on the fractograph of the samples, which indicate good capability of plastic deformation exists in the samples (Figure 8b, Figure 8d, Figure 8f and Figure 8h). Yin et al. and Hu et al. have proven the similar fractograph morphologies for the brittle fracture (transgranular cleavage plane) and the ductile fracture (dimples) of the Ti-6Al-4V alloy tested in methanol solution and air condition during the slow strain rate test [46,52].

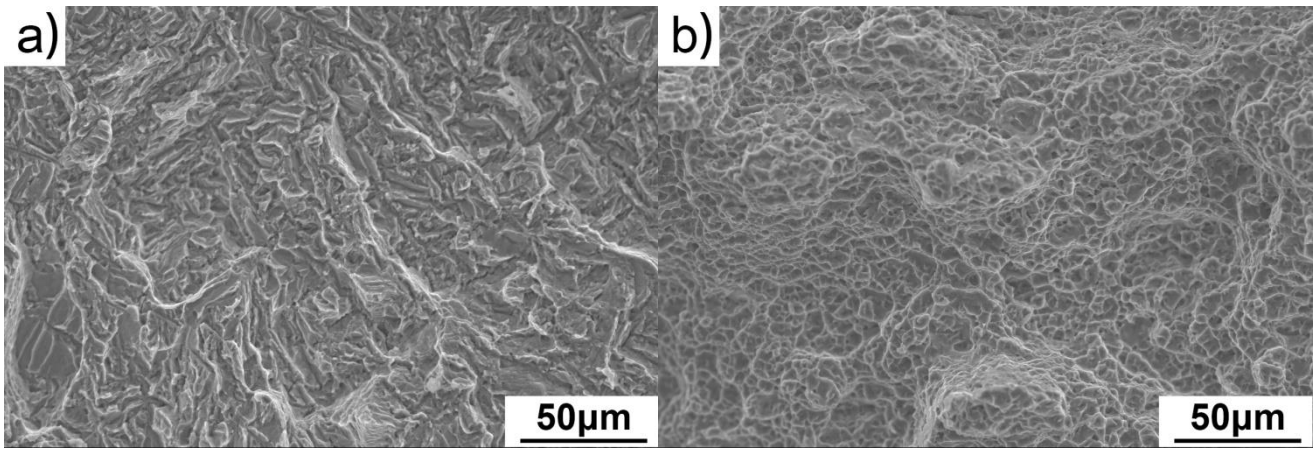

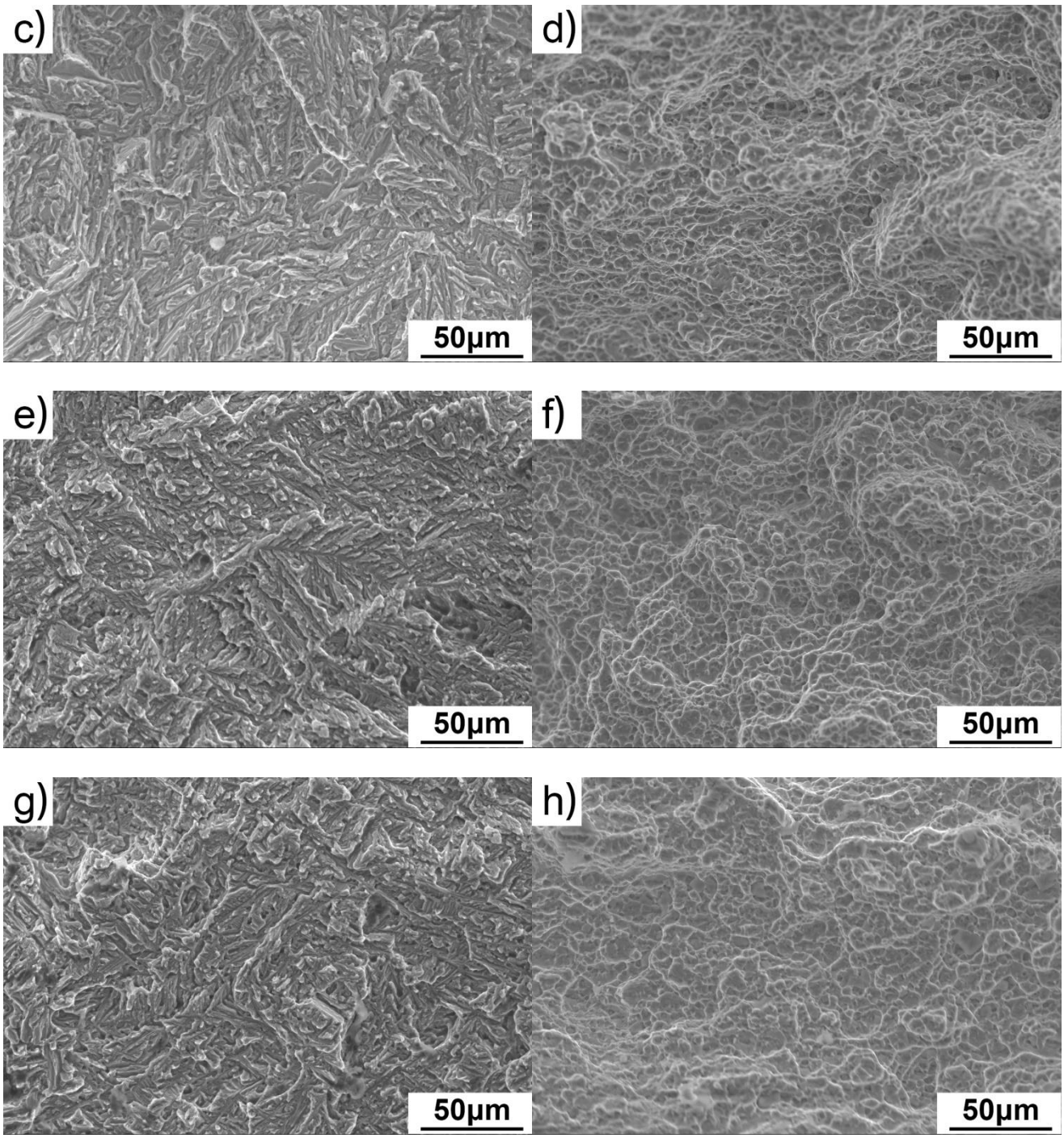

Figure 8. Fractograph of the as-welded and the heat treated samples with the different temperatures: (a), (b) as-welded sample tested in solution and air; (c), (d) 910 ℃ treated sample tested in solution and air; (e), (f) 940 ℃ treated sample tested in solution and air; (g), (h) 970 ℃ treated sample tested in solution and air.

3.3 Electrochemical impedance spectroscopy analysis with the slow strain rate test test

Figure 9 displays the evolution of the electrochemical impedance spectroscopy of the welded samples before and after heat treatment during the slow strain rate test process. It is clear that there is an identical feature for all the impedance spectroscopy, the Nyquist plots are featured with a

capacitance loop over the whole tested frequency range, which clearly presents one time constant in the measurement process. The radius of the capacitance loop decreases continuously with the increase in the immersion time.

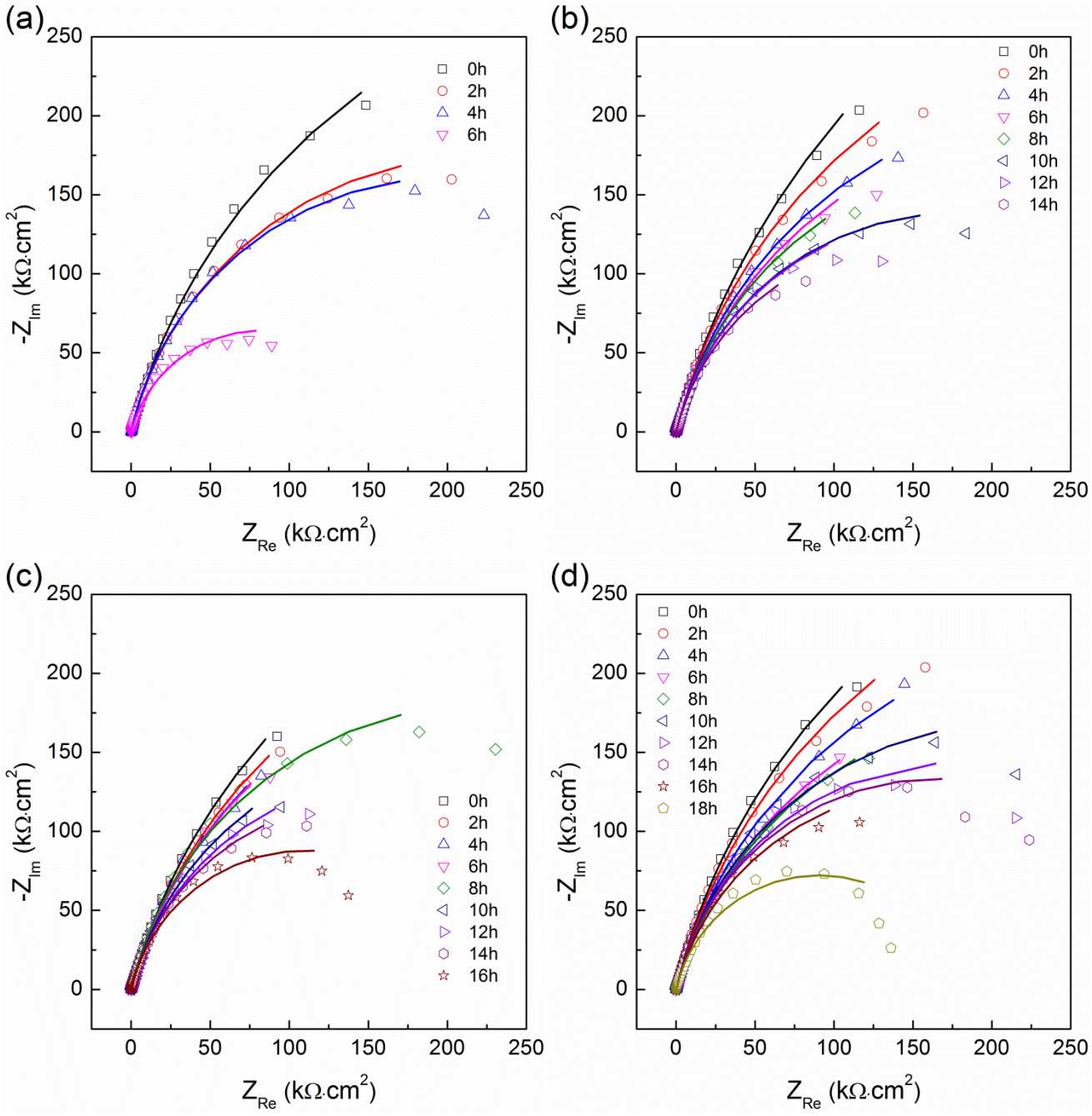

Figure 9. Evolution of the electrochemical impedance spectroscopy of the as-welded and the heat treated samples with the different temperatures during the slow strain rate test process (symbols are experimental data and solid lines are fitting data): (a) as-welded sample [17]; (b) 910 ℃ treated sample; (c) 940 ℃ treated sample; (d) 970 ℃ treated sample.

The EIS results can be fitted by using the equivalent circuit model which is shown in Figure 10. In this equivalent circuit model, there is only one time constant, where R_s is the solution resistance, Q_{dl} is the constant phase element for the electrochemical double layer and the R_{ct} is the charge transfer resistance. The equivalent circuit has been widely used to describe the corrosion behavior for titanium alloy in various corrosive medium such as simulated physiological condition (Ringer's solution) and simulated sea water condition (3.5% NaCl solution), and the equivalent circuit R_s (Q_{dl} R_{ct}) which is shown in Figure 10 has been proven to be suitable and accurate for the corrosion behavior of titanium alloy [53-55]. There is a good correspondence (shown in Figure 9) between the fitted (solid lines) and the measured (symbols) spectroscopy, which indicates a low fitting error and good data accuracy of the fitting result. The fitting results are exhibited in Table 5, 6, 7 and 8.

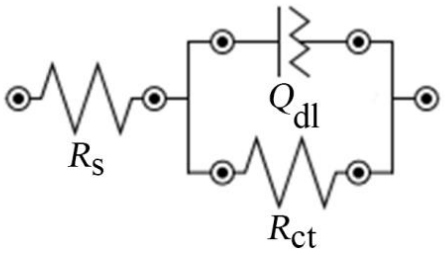

Figure 10. Equivalent circuit models for the electrochemical impedance spectroscopy of the as-welded and heat treated samples during the slow strain rate test process.

Table 5. EIS fitting parameters for the as-weld sample.

Time (h)	R_s ($\Omega \cdot cm^2$)	Q_{dl} ($\Omega^{-1} \cdot S^n \cdot cm^{-2}$)	n	R_{ct} ($\Omega \cdot cm^2$)
0	36.58	3.362×10^{-5}	0.8392	7.461×10^5
2	36.87	3.171×10^{-5}	0.8499	4.412×10^5
4	34.59	3.288×10^{-5}	0.8646	3.976×10^5
6	36.93	3.682×10^{-5}	0.8414	1.647×10^5

Table 6. EIS fitting parameters for the 940 ℃ treated sample.

Time (h)	R_s ($\Omega \cdot cm^2$)	Q_{dl} ($\Omega^{-1} \cdot S^n \cdot cm^{-2}$)	n	R_{ct} ($\Omega \cdot cm^2$)
0	35.62	4.221×10^{-5}	0.8351	8.621×10^5
2	35.57	4.304×10^{-5}	0.8332	6.211×10^5
4	36.71	3.248×10^{-5}	0.8451	5.331×10^5
6	36.37	3.888×10^{-5}	0.8298	4.991×10^5
8	36.75	3.589×10^{-5}	0.8432	4.476×10^5
10	34.93	3.489×10^{-5}	0.8511	3.494×10^5
12	36.32	3.726×10^{-5}	0.8508	3.445×10^5
14	36.99	3.508×10^{-5}	0.8486	3.031×10^5

Table 7. EIS fitting parameters for the 940 ℃ treated sample.

Time (h)	R_s ($\Omega \cdot cm^2$)	Q_{dl} ($\Omega^{-1} \cdot S^n \cdot cm^{-2}$)	n	R_{ct} ($\Omega \cdot cm^2$)
0	35.75	4.091×10^{-5}	0.8376	8.698×10^5
2	36.16	3.833×10^{-5}	0.8471	6.815×10^5
4	32.26	4.151×10^{-5}	0.8311	5.736×10^5
6	31.96	3.947×10^{-5}	0.8355	5.049×10^5
8	32.91	3.254×10^{-5}	0.8608	4.491×10^5
10	36.86	3.592×10^{-5}	0.8437	3.958×10^5
12	32.71	3.841×10^{-5}	0.8385	3.479×10^5
14	36.91	3.571×10^{-5}	0.8451	3.095×10^5
16	37.31	3.085×10^{-5}	0.8561	2.207×10^5

Table 8. EIS fitting parameters for the 970 ℃ treated sample.

Time (h)	R_s ($\Omega \cdot cm^2$)	Q_{dl} ($\Omega^{-1} \cdot S^n \cdot cm^{-2}$)	n	R_{ct} ($\Omega \cdot cm^2$)
0	34.26	3.582×10^{-5}	0.8517	9.014×10^5
2	36.11	3.872×10^{-5}	0.8457	7.021×10^5
4	36.45	3.673×10^{-5}	0.8389	5.811×10^5
6	32.34	4.046×10^{-5}	0.8312	5.662×10^5
8	35.51	4.423×10^{-5}	0.8307	4.631×10^5
10	34.87	3.317×10^{-5}	0.8551	4.231×10^5
12	34.72	3.343×10^{-5}	0.8607	3.577×10^5
14	34.75	3.255×10^{-5}	0.8661	3.293×10^5
16	36.43	3.662×10^{-5}	0.8411	3.261×10^5
18	36.99	3.271×10^{-5}	0.8573	1.811×10^5

As the fitting results show, there are obvious differences in the charge transfer resistance between the as-welded sample and the heat treated samples. It is seen that the charge transfer resistance of the as-welded sample and the heat treated samples presents a continuous decline during the slow strain rate test process. The charge transfer resistance of the welded samples is observed to obviously increase after the heat treatment, thus, the corrosion resistance of the welded samples is significantly improved by the post weld heat treatment due to the proportional relationship between the charge transfer resistance and the corrosion resistance of the samples.

It is seen that the Nyquist plots of the electrochemical impedance spectroscopy of the as-welded and heat treated samples present the identical feature (only one capacitance loop), which indicates that the changes of the microstructures do not alter the electrochemical mechanism of the stress corrosion cracking, but the corrosion resistance of the welded sample can be improved by the post weld local rapid induction heating.

From the above, it is suggested that the post weld heat treatment affects the stress corrosion cracking behavior and the electrochemical behaviors of the welded samples by improving the microstructure in the fusion zone. The microstructure results show that the phase transformation $\alpha + \beta \rightarrow \alpha' \rightarrow \alpha + \beta$ occurs in the fusion zone when the alloy undergoes welding and post weld heat treatment, in addition, the content of the β phases in the fusion zone gradually increase with the heat treatment temperature. The slow strain rate test and electrochemical impedance spectroscopy indicate that the mechanical property, susceptibility index of stress corrosion cracking and corrosion resistance

of the samples are significantly improved through the post weld heat treatment, and the higher heat treatment temperature implies the better mechanical property, lower susceptibility index of stress corrosion cracking and higher corrosion resistance of the samples. From the results of microstructure, slow strain rate test and electrochemical impedance spectroscopy, it is quite clear that the acicular α′ martensite phase which is caused by the welding process is susceptible and the β phase is immune to the stress corrosion cracking, the β phase plays a role as crack arrester during the stress corrosion cracking process. Thus, the susceptibility of the welded samples to the stress corrosion cracking can be reduced by transforming the susceptible α′ martensite phase and increasing the content of the immune β phase.

In summary, it can be seen that the fracture time, break strength and corrosion resistance of the welded Ti-6Al-4V alloy during slow strain rate test are significantly enhanced by the heat treatment, which increase with the increase of the heat treatment temperature in this study. It indicates that the post weld heat treatment is capable to enhance the resistance of the welded Ti-6Al-4V alloy to stress corrosion cracking effectively.

3.4 Kramers-Kronig transformation

In order to verify the validity of the experimental electrochemical impendence data, Kramers-Kronig transformation is used in this study. Kramers-Kronig transformations of the experimental data are exhibited in Figure 11. As can be seen, Kramers-Kronig transformations fit the experimental data quite well over the tested frequency range.

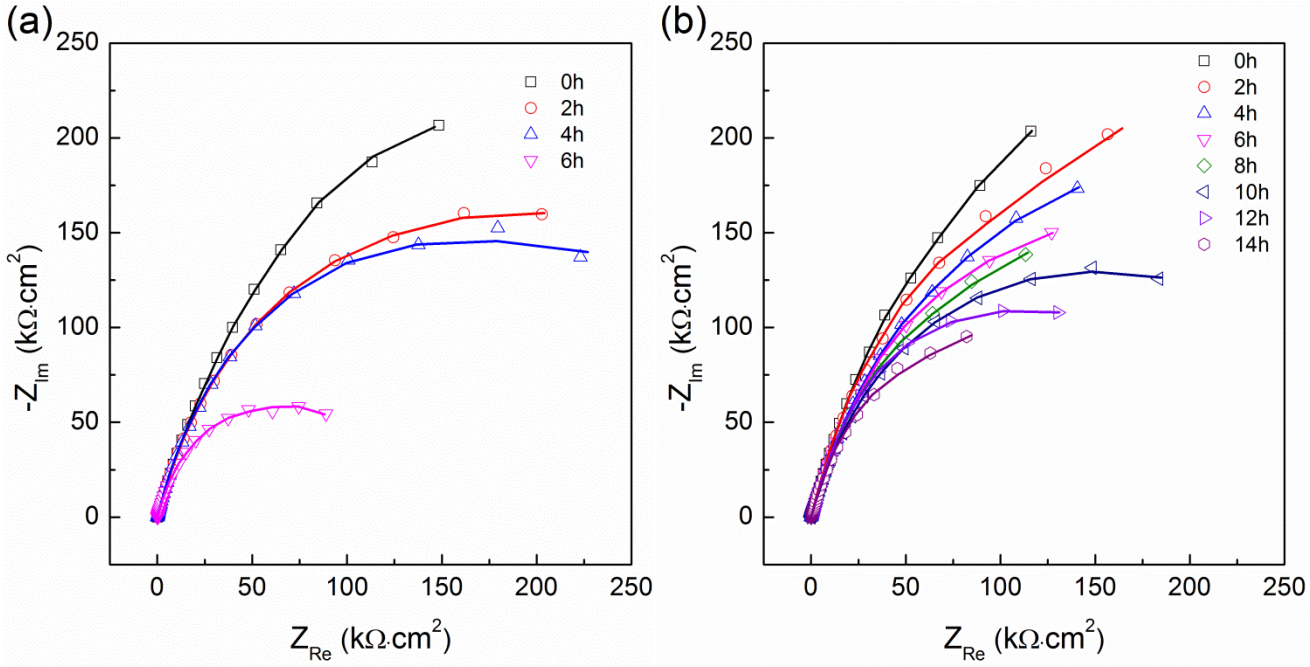

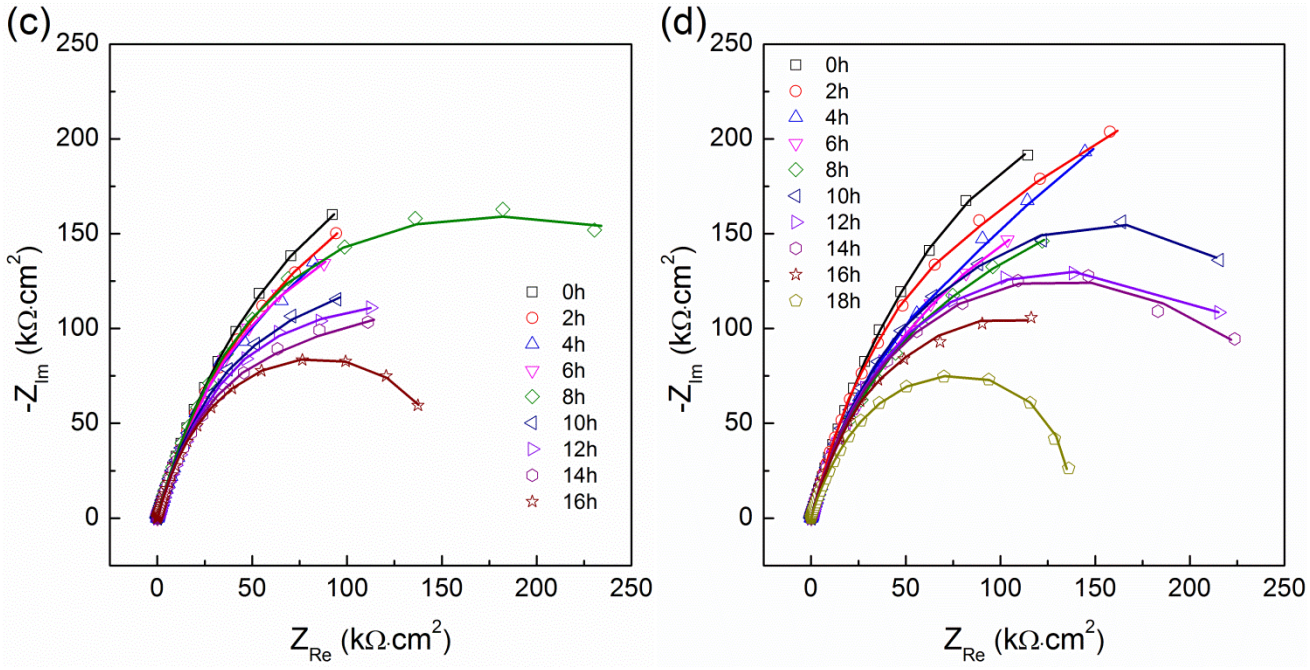

Figure 11. Kramers-Kronig transformation of the electrochemical impedance spectroscopy of the as-welded and the heat treated samples with the different temperatures during the slow strain rate test process (symbols are experimental data and solid lines are fitting data): (a) as-welded sample [17]; (b) 910 ℃ treated sample; (c) 940 ℃ treated sample; (d) 970 ℃ treated sample.

4. CONCLUSIONS

The stress corrosion cracking resistance of the welded Ti-6Al-4V alloy is improved by the post weld local rapid induction heating. The effect of the heat treatment on the stress corrosion cracking behavior and electrochemical characteristic has been discussed. The results are summarized as follows:

(1) The microstructure of the fusion zone transforms from the acicular α′ martensite phase to the lathy α phase and the transformational β phase after the post weld local rapid induction heating. The increase of the heat treatment temperature causes the content of the lathy α phase to decrease and the content of the transformational β phase to increase in the fusion zone.

(2) The mechanical properties of the welded samples are obviously improved after the heat treatment, which increase with the heat treatment temperature of the post weld heat treatment under the slow strain rate test. Compared with the as-welded sample, the ultimate tensile strength and breaking elongation of the welded sample are increased by 168 % and 175 % after the post weld heat treatment at 970 ℃, respectively. The susceptibility index of the stress corrosion cracking significantly decreases after the heat treatment and the higher heat treatment temperature implies the lower susceptibility index.

(3) The radius of the capacitance loop continuously decreases for all the samples during the electrochemical impedance spectroscopy measurements process under the slow strain rate test. The post weld heat treatment can effectively enhances the corrosion resistance of the welded sample, and the corrosion resistance increases with the increase of the heat treatment temperature.

(4) The microstructure in the fusion zone plays an important role in the stress corrosion cracking behavior of the welded Ti-6Al-4V alloy. After the heat treatment, the susceptibility of the welded Ti-6Al-4V alloy to the stress corrosion cracking can be significantly reduced through transforming the α′ martensite phase to the α phase and the β phase, and increasing the content of the β phase.

References

1. R. M. A. Shahba, W. A. Ghannem, A. El-Sayed. El-Shenawy, A. S. I. Ahmed, S. M. Tantawy, *Int. J. Electrochem. Sci*. 6 (2011) 5499.
2. J. Mendoza-Canales, J. Marín-Cruz, *Int. J. Electrochem. Sci*. 3 (2008) 346.
3. C. G. Nava-Dino, R. G. Bautista-Margulis, M. A. Neri-Flores, M. V. Orozco-Carmona, S. D. Torre, J. G. Gonzalez-Rodriguez, J. G. Chacon-Nava, A. Martínez-Villafañe, *Int. J. Electrochem. Sci*. 7 (2012) 4250.
4. C. G. Nava-Dino, C. López-Meléndez, R. G. Bautista-Margulis, M. A. Neri-Flores, J. G. Chacon-Nava, S. D. Torre, J. G. Gonzalez-Rodriguez, A. Martínez-Villafañe, *Int. J. Electrochem. Sci*. 7 (2012) 2389.
5. C. Vasilescu, P. Drob, E. Vasilescu, P. Osiceanu, S. I. Drob, M. V. Popa, *Int. J. Electrochem. Sci*. 8 (2013) 10733.
6. B. Tang, P. Q. Wu, A. L. Fan, L. Qin, H. J. Hu, J. P. Celis, *Adv. Eng. Mater*. 7 (2005) 232.
7. S. A. Fadl-allah, Q. Mohsen, *Appl. Surf. Sci*. 256 (2010) 5849.
8. D. Mareci, R. Chelariu, A. Cailean, F. Brinza, G. Bolat, D.M. Gordin, *Trans. Nonferrous Met. Soc. China*. 25 (2015) 345.
9. A. L. Pilchak, A.H. Young, J.C. Williams, *Corros. Sci*. 52 (2010) 3287.
10. S. P. Trasatti, E. Sivieri, *Mater. Chem. Phys*. 83 (2004) 367.
11. M. D. Pustode, V.S. Raja, N. Paulose, *Corros. Sci*. 82 (2014) 191.
12. W. T. Tsai, C. L. Lin, S. J. Pan, *Corros. Sci*. 76 (2013) 494.
13. X. L. Gao, L. J. Zhang, J. Liu, J. X. Zhang, *Mat. Sci. Eng. A-Struct*. 559 (2013) 14.
14. H. Liu, K. Nakata, N. Yamamoto, *J. Mater. Sci*. 47 (2012) 1460.
15. P. Q. Xu, L. Li, C. Zhang, *Mater. Charact*. 87 (2014) 179.
16. F. Karimzadeh, M. Heidarbeigy, A. Saatchi, *J. Mater. Process. Tech*. 206 (2008) 388.
17. M. Heidarbeigy, F. Karimzadeh, A. Saatchi, *Mater. Lett*. 62 (2008) 1575.
18. Z. Han, H. Zhao, X. Y. Chen, H. C. Lin, *Mat. Sci. Eng. A-Struct*. 277 (2000) 38.
19. Y. Liu, S. W. Tang, G. Y. Liu, Y. Sun, J. Hu, *Int. J. Electrochem. Sci*. in press (2016).
20. S. Ghosh, V. P. S. Rana, V. Kain, V. M, S. K. Baveja, *Mater. Design*. 32 (2011) 3823.
21. M. Mochizuki, *Nucl. Eng. Des*. 237 (2007) 107.
22. A. S. H. Kabir, X. J. Cao, J. Gholipour, P. Wanjara, J. Cuddy, A. Birur, M. Medraj, *Metall. Mater. Trans. A*. 43 (2012) 4171.
23. G. Thomas, V. Ramachandra, R. Ganeshan, *J. Mater. Sci*. 28 (1993) 4892.
24. C. C. Zhang, T. C. Zhang, Y. J. Ji, J. H. Huang, *Trans. Nonferrous Met. Soc. China*. 23 (2013) 3540.
25. J. Komotori a, M. Shimizu a, Y. Misaka , K. Kawasaki, *Int. J. Fatigue*. 23 (2001) 225.
26. M. Dewidar, *Mater. Design*. 31 (2010) 3964.
27. P. E. Markovskya, S. L. Semiatinb, *J. Mater. Process. Tech*. 210 (2010) 518.
28. S. L. Semiatin, S. L. Knisley, P. N. Fagin, F. Zhang, D. R. Barker, *Metall. Mater. Trans. A*. 34 (2011) 2377.
29. P. E. Markovskya, S. L. Semiatinb, *Mat. Sci. Eng. A-Struct*. 528 (2011) 3079.
30. M. Atapour, M. H. Fathi, M. Shamanian, *Mater. Corros*. 63 (2012) 134.

31. K. Hagihara, M. Okubo, M. Yamasaki, T. Nakano, *Corros. Sci*. 2016.
32. Y. Wang, W. Zhao, H. Ai, X. Zhou, T. Zhang, *Corros. Sci*. 53 (2011) 2761.
33. A. A. Oskuie, T. Shahrabi, A. Shahriari, E. Saebnoori, *Corros. Sci*. 61 (2012) 111.
34. M. Sun, K. Xiao, C. Dong, X. Li, P. Zhong, *Corros. Sci*. 89 (2014) 137.
35. S. Sunada, N. Nunomura, *Arch. Metall. Mater*. 58 (2013) 505.
36. C. S. Brossia, E. Gileadi, R. G. Kelly, *Corros. Sci*. 37 (1995) 1455.
37. T. Kawai, H. Nishisara, K. Aramaki, *Corros. Sci*. 37 (1995) 823.
38. T. Kawai, H. Nishisara, K. Aramaki, *Corros. Sci*. 8 (1996) 225.
39. C. S. Brossia, R. G. Kelly, *Electrochim. Acta*. 41 (1996) 2579.
40. T. Kawai, H. Nishihara, K. Aramaki, *J. Electrochem. Soc*. 143 (1996) 3866.
41. G. Thomas, V. Ramachandra, M. J. Nair, K. V. Nagarajan, R. Vasudevan, *Weld. J*. 1 (1992) 15.
42. N. Winzer, A. Atrens, G. L. Song, E. Ghali, W. Dietzel, K. U. Kainer, N. Hort, C. Blawert, *Adv. Eng. Mater*. 7 (2005) 659.
43. A. Atrens, N. Winzer, W. Dietzel, *Adv. Eng. Mater*. 13 (2011) 11.
44. E. Aghion, I. Guinguis, *Adv. Eng. Mater*. 11 (2009) 920.
45. A. Arnon, E. Aghion, *Adv. Eng. Mater*. 10 (2008) 742.
46. J. O. Yin, Y. S. Wu, J. Lu, B. F. Ding, L. Zhang, B. Cao, *Rare. Metal. Mat. Eng*. 6 (2003) 436.
47. C. J. O. Alonso1, J. G. G. Rodriguez, J. U. Chavarin1, J. G. C. Nava, *Int. J. Electrochem. Sci*. 10 (2015) 5249.
48. H. Zhang, X. D. Wang, R. L. Jia, J. Hou, W. M. Guo, *Int. J. Electrochem. Sci*. 8 (2015) 1262.
49. M. D. Pustode, V. S. Raja, *Metall. Mater. Trans. A*. 46 (2015) 6081.
50. Y. S. Wu, Y. L. Jiang, H. Chu, Z. Y. Ding, B. F. Ding, *J. Univ. Sci. Technol. B*. 1 (2003) 40.
51. M. Mihalikova, M. Hagarova, D. Jakubéczyová, J. Cervová, A. Lišková, *Int. J. Electrochem. Sci*. 11 (2016) 4206.
52. M. J. Hu, H. J. Liu, *Trans. Nonferrous Met. Soc. China*. 19 (2009) 324.
53. J. E. G. Gonza´lez, J. C. M. Rosca, *J. Electroanal. Chem*. 471 (1999) 109.
54. C. H. Zhang, W. Song, F. B. Li, X. Zhao, Y. M. Wang, G. Z. Xiao, *Int. J. Electrochem. Sci*. 10 (2015) 9167.
55. R. Ittah, I. Malka, I. Bar, D. Itzhak, *Int. J. Electrochem. Sci*. 10 (2015) 1326.